

Topological thermal Hall effect driven by fluctuation of spin chirality in frustrated antiferromagnets

Yalei Lu¹, Xing Guo¹, Vladimir Koval², and Chenglong Jia^{1,3*}

¹Key Laboratory for Magnetism and Magnetic Materials of MOE, Lanzhou University, 730000 Lanzhou, China

²Institute of Materials Research, Slovak Academy of Sciences, Watsonova 47, 04001 Kosice, Slovakia

³Institut für Physik, Martin-Luther Universität Halle-Wittenberg, 06099 Halle (Saale), Germany

(Dated: March 10, 2024)

By revealing an underlying relation between the Dzyaloshinskii-Moriya interaction (DMI) and the scalar spin chirality, we have developed the theory of magnon thermal Hall effects in antiferromagnetic systems. The dynamic fluctuation of the scalar chirality is shown to directly respond to the nontrivial topology of magnon bands. In materials such as the jarosites compounds $\text{KFe}_3(\text{OH})_6(\text{SO}_4)_2$ and veseignite $\text{BaCu}_3\text{V}_2\text{O}_8(\text{OH})_2$ in the presence of in-plane DMI, the time-reversal symmetry can be broken by the fluctuations of scalar chirality even in the case of coplanar $\mathbf{q} = 0$ magnetic configuration. The spin-wave Hamiltonian is influenced by a fictitious magnetic flux determined by the in-plane DMI. Topological magnon bands and corresponding nonzero Chern numbers are presented without the need of a canted non-coplanar magnetic ordering. The canting angle dependence of thermal Hall conductivity is discussed in detail as well. These results provide a clear principle of chirality-driven topological effects in antiferromagnetically coupled systems.

I. INTRODUCTION

Topological excitations of quantum matter are the subject of extensive interest in condensed matter physics. They have been theoretically predicted and experimentally observed in electron systems [1–5]. Topological band structure of electrons can be probed by the Hall effect, linked to the Berry curvature throughout the Brillouin zone [6, 7]. In principle, the concept of topological band theory is independent of the statistical nature of (quasi-)particles. Therefore, the concepts of topological excitations can be extended to neutral bosonic systems such as photons [8–10], phonons [11–16], and magnons [17–35]. For spin systems, the magnons do not experience a Lorentz force, which usually drives the electronic Hall effects, but a thermal version of the Hall effect induced by a temperature gradient [17]. The thermal Hall effect has been confirmed experimentally in insulating pyrochlore [18] and kagome ferromagnets [24, 25].

Ordered magnetic insulators with topological magnons as the analogue of Chern insulators requires inherently to break time-reversal symmetry (TRS) [1]. In the most cases without applied external magnetic fields, the TRS-broken state is closely related to the (scalar) spin chirality $\hat{\chi}_{ijk} = \mathbf{S}_i \cdot (\mathbf{S}_j \times \mathbf{S}_k)$ [36, 37]. For ferromagnets, Katsura *et al.* showed that the scalar spin chirality, emerging in the form of ring exchange, provides a fictitious magnetic field for the magnons [17]. In the low temperature limit, the thermal Hall conductivity κ_{xy} is found to be linearly dependent on the fictitious magnetic flux. In Refs. [26, 38], Lee *et al.* generalized the intimate connection between the spin chirality and the Hall-like transport in purely spin systems (including paramagnetic and spin-liquid regimes) based on the linear response theory. On

the other hand, for antiferromagnets such as frustrated kagome magnets, a *noncoplanar* spin configuration with *finite* averaged scalar spin chirality $\langle \hat{\chi}_{ijk} \rangle$ breaks TRS spontaneously and macroscopically and is believed to respond to the nontrivial topology and the corresponding magnon Hall effect [39, 40]. However, a large magnon thermal Hall conductivity can be found even when the scalar spin chirality is very small [41]. This contradictory phenomena suggests that, unlike the cases of ferromagnets, the role of the spin chirality on magnon Hall effects in antiferromagnets still remains puzzling in many aspects.

In the present study, we show that the coplanar $\mathbf{q} = 0$ magnetic structure on kagome antiferromagnets can give a finite thermal Hall effect if the in-plane Dzyaloshinskii-Moriya interaction (DMI) exists. It is obviously that the non-coplanar spins with finite scalar chirality can't be regarded as the single source of topological magnon bands in frustrated antiferromagnets. One needs to investigate the underlying mechanism in more depth. Here we consider magnetically ordered insulating systems, the thermal transport is mainly carried by the quantized spin fluctuations (magnons). Therefore, it is worthwhile to conduct an investigation into the fluctuation of the scalar chirality up to the second order in $\delta \mathbf{S}_i = \mathbf{S}_i - \langle \mathbf{S}_i \rangle$, i.e., $\delta \hat{\chi}_{ijk} = \langle \mathbf{S}_i \rangle \cdot (\delta \mathbf{S}_j \times \delta \mathbf{S}_k)$, which is more relevant to magnonic transport than does the scalar chirality $\langle \hat{\chi}_{ijk} \rangle$. Moreover, even if the scalar chirality $\langle \hat{\chi}_{ijk} \rangle = 0$, the fluctuation $\delta \hat{\chi}_{ijk}$ can have a finite value and break dynamically the TRS, leading to topological magnons. Similar to previous studies [17, 39, 41], we examine the DMI term $\mathbf{D}_{jk} \cdot (\mathbf{S}_j \times \mathbf{S}_k)$, which is rewritten to include an effective ring exchange interaction of three neighbouring spins, $\sim K_\Phi/S [\mathbf{S}_i \cdot (\mathbf{S}_j \times \mathbf{S}_k)]$ and to introduce explicitly $\delta \hat{\chi}_{ijk}$ to the spin-wave Hamiltonian. We show that the component of DM vector (\mathbf{D}_{jk}) parallel to the $\langle \mathbf{S}_i \rangle$ can lead to a finite magnetic flux K_Φ and nontrivial topological effects. The perpendicular component, however, is

* cljia@lzu.edu.cn

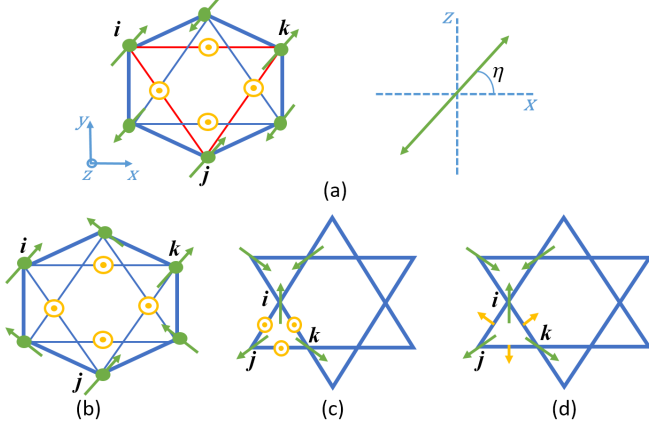


FIG. 1. (a) The honeycomb lattice with collinear order (left). The DMI (yellow circle) points out-of-plane at the midpoint of the next-nearest-neighbour bonds. The angle between the collinear spin moment and the honeycomb plane is indicated by η (right). (b) The honeycomb lattice with non-collinear order. DMI is same as in (a). (c) Coplanar $\mathbf{q} = 0$ spin configuration on the kagome lattice with positive vector chirality. DMI (yellow circle) is perpendicular to the kagome plane at the midpoint of the nearest-neighbour bonds. (d) Coplanar $\mathbf{q} = 0$ spin configuration on the kagome lattice with positive vector chirality. DMI (yellow arrow) lies in the kagome plane and is perpendicular to the midpoint of the nearest-neighbour bonds. The green arrows indicate the directions of spins.

irrelevant to the thermal Hall effect. Analogous to ferromagnetic systems, the principle (no-go theorem) [17] is generalised to rule out the magnon thermal Hall effect in coupled antiferromagnetic systems.

The article is organised as follows. In Sec. II we explicitly give out the relation between the DMI and the fluctuation of spin chirality, and emphasize the importance of effective magnetic flux $K_\Phi \sim \langle \mathbf{D}_{jk} \cdot \mathbf{S}_i \rangle$. We show that the (exactly) coplanar spin configuration with an in-plane DMI can give rise to a non-zero K_Φ and induce the nontrivial topology. In Sec. III we introduce the spin model with the in-plane DMI for the kagome antiferromagnets and substantiate the topological nature of magnon bands based on the Holstein-Primakoff method. In Sec. IV the thermal Hall conductivity is calculated with different canting angles. Conclusions and discussions are given in Sec. V.

II. DZIALOSHINSKII-MORIYA INTERACTION AND SPIN CHIRALITY

As pointed out by Katsura *et al.* in Ref. [17], there is a coupling between the scalar chirality and magnetic fields through the ring exchange process, which, we believe, is the primary interaction source of magnon topological effects in spin systems. In order to get such TRS-broken

three-spin interactions in a spin Hamiltonian with the (two-spin) DMI, we decompose the DM vector as,

$$\mathbf{D}_{ij} = \mathbf{D}_{ij}^\perp + \mathbf{D}_{ij}^\parallel, \quad (1)$$

where $\mathbf{D}_{ij}^\parallel$ represents the component whose direction aligns with the third contiguous spin \mathbf{S}_k that is determined uniquely through the (cyc. perm.) triangular-bond Δ_{ijk} . \mathbf{D}_{ij}^\perp describes the transverse deviation from \mathbf{S}_k . If $\mathbf{D}_{ij}^\parallel \neq 0$, the DMI can be mapped effectively onto a ring exchange interaction as,

$$\mathbf{D}_{ij}^\parallel \cdot (\mathbf{S}_i \times \mathbf{S}_j) = \frac{K_\Phi}{S} \mathbf{S}_k \cdot (\mathbf{S}_i \times \mathbf{S}_j), \quad (2)$$

where $K_\Phi = \mathbf{D}_{ij} \cdot \mathbf{S}_k / S$. The DM vector behaves as an “orbital magnetic field” in Eq. (2). For example, in the collinear ferromagnetic kagome systems, all spin moments are given to be directed normal to the kagome plane and only the out-of-plane DMI is considered $\mathbf{D}_{ij} = \mathbf{D}_z$, one has $K_\Phi = D_z \neq 0$ and then finite magnon Hall-type transport [17, 24, 25]. However, the fictitious magnetic flux K_Φ does not always exist due to the dot product between \mathbf{D}_{ij} and \mathbf{S}_k , especially in the antiferromagnetic systems.

As an example, let’s revisit the antiferromagnetic honeycomb lattice with out-of-plane DMI, as shown in Fig. 1(a). In the case of collinear spins, the DMI of six bonds can be classified into two classes (corresponding the blue \triangle and red ∇ in Fig. 1(a),

$$\mathbf{D}_z \cdot (\mathbf{S}_i \times \mathbf{S}_j)_{\nabla} \Rightarrow \frac{D_z}{S} \sin(\eta) \langle \mathbf{S}_k \rangle \cdot (\delta \mathbf{S}_i \times \delta \mathbf{S}_j), \quad (3)$$

$$\mathbf{D}_z \cdot (\mathbf{S}_i \times \mathbf{S}_j)_{\triangle} \Rightarrow -\frac{D_z}{S} \sin(\eta) \langle \mathbf{S}_k \rangle \cdot (\delta \mathbf{S}_i \times \delta \mathbf{S}_j), \quad (4)$$

where η is the angle between the spin plane and the honeycomb plane. Clearly, the scalar chirality fluctuation of upward-pointing triangle \triangle cancels out the contribution from the downward-pointing triangle ∇ . No matter which value η takes, one always has the total $K_\Phi = 0$, which implies that the out-of-plane DMI can’t serve as the coupling field in the spin-wave Hamiltonian. However, for the case with non-collinear spin configuration as shown in Fig. 1(b), the cancellation doesn’t occur,

$$\mathbf{D}_z \cdot (\mathbf{S}_i \times \mathbf{S}_j)_{\nabla} \Rightarrow \frac{D_z}{S} \sin(\eta) \langle \mathbf{S}_k \rangle \cdot (\delta \mathbf{S}_i \times \delta \mathbf{S}_j), \quad (5)$$

$$\mathbf{D}_z \cdot (\mathbf{S}_i \times \mathbf{S}_j)_{\triangle} \Rightarrow \frac{D_z}{S} \sin(\eta) \langle \mathbf{S}_k \rangle \cdot (\delta \mathbf{S}_i \times \delta \mathbf{S}_j), \quad (6)$$

where η is redefined for the angle between the corresponding spin moment $\langle \mathbf{S}_k \rangle$ and the honeycomb plane. Now $K_\Phi \propto \sin(\eta)$, which deduces that the thermal Hall conductivity is proportional to the canting angle η , in consistent with the previous results [42]. Similarly, the coupling magnetic flux in kagome antiferromagnets with

TABLE I. Connection between the spin chirality and the thermal Hall effects in honeycomb and kagome lattices with out-of-plane DMI \mathbf{D}_z .

	Magnetic structure	Fictitious magnetic flux K_Φ	Ref.	Thermal Hall coefficient κ_{xy}	Mechanism
Honeycomb	Collinear FM	D_z	[28, 30]	$\sim D_z$	DMI
	Collinear AFM	0	[42]	0	no
	Canted non-collinear AFM	$D_z \sin(\eta)$	[42]	$\sim D_z \sin(\eta)$	DMI and Zeeman field
Kagome	Collinear FM	D_z	[17, 43]	D_z	DMI
	Coplanar $\mathbf{q} = 0$ 120° AFM	0	[40]	0	no
	Non-coplanar 120° AFM	$(J + D_z) \sin(\eta)$	[40]	$\sim (J + D_z) \sin(\eta)$	Non-coplanar chiral spin

the out-of-plane DMI and the coplanar $\mathbf{q} = 0$ state is zero because of the orthogonality between the DM vector \mathbf{D}_z and adjacent spin \mathbf{S}_k (cf. Fig. 1(c)). For comparison, in Table I, we list topological properties of different spin configurations on honeycomb/kagome lattices in terms of the fictitious magnetic flux, along with previous studies in the literature.

Now we turn to the research on the effect of in-plane DMI (\mathbf{D}_p). For the coplanar $\mathbf{q} = 0$ spin configuration on the kagome lattice (as shown in Fig. 1(d)), the magnetic flux provided by the in-plane DMI can survive since the \mathbf{D}_p is parallel to $\langle \mathbf{S}_k \rangle$,

$$\mathbf{D}_p \cdot (\mathbf{S}_i \times \mathbf{S}_j) \Rightarrow -\frac{D_p}{S} \langle \mathbf{S}_k \rangle \cdot (\delta \mathbf{S}_i \times \delta \mathbf{S}_j). \quad (7)$$

Noted that the sign in Eq. (7) is opposite to the contribution given by the non-zero scalar chirality [40]. Consequently the coupling fields provided respectively by the in-plane DMI and the scalar chirality will weaken each other (in the Sec. IV we will discuss this cancellation in more detail). From the symmetry point of view, the so-called (non-coplanar) umbrella spins with non-zero scalar chirality $\langle \chi_{ijk} \rangle \neq 0$ and a weak ferromagnetic moment breaks the TRS statically [41, 44, 45]. However, the fluctuation of scalar chirality $\delta \chi_{ijk}$ can be finite from the mean-field argument even though $\langle \chi_{ijk} \rangle = 0$ in the case of coplanar magnetic orders, Eq. (7) suggests a dynamically TRS-broken interaction in the spin-wave Hamiltonian. A finite topological magnon Hall effect is thus expected in the coplanar spin configuration with the in-plane DMI.

III. SPIN MODEL AND TOPOLOGICAL MAGNONS

Let's consider the spin model on the frustrated kagome lattice, in which the DMI comes naturally because of lacking of an inversion center [46, 47],

$$H = \sum_{i,j} J_{ij} \mathbf{S}_i \cdot \mathbf{S}_j - \sum_{(i,j)} \mathbf{D}_{ij} \cdot \mathbf{S}_i \times \mathbf{S}_j - B \hat{\mathbf{z}} \cdot \sum_i \mathbf{S}_i, \quad (8)$$

where the first term contains the nearest-neighbour (NN) and the next-nearest-neighbour (NNN) antiferro-

magnetic interactions J_1 and J_2 , respectively. $\mathbf{D}_{ij} = (0, D_p, D_z)$ with D_p and D_z being the in-plane and the out-of-plane DMI for the bond (ij) , respectively (cf. Fig. 2). \mathbf{B} is the normal magnetic field in units of $g\mu_B$. The influence of the DMI in the frustrated kagome lattice has been studied extensively. For the spin-1/2 case, both exact diagonalization method and the Schwinger bosons mean field theory have predicted a quantum transition between the quantum spin liquid with a small $|D_z|$ and the $\mathbf{q} = 0$ Néel state as $|D_z| > D_z^c \approx 0.1J_1$ [48–52]. For higher spins, an ordered 120° magnetic configuration is favorite in energy [44]. The out-of-plane DMI D_z stabilizes the 120° coplanar $\mathbf{q} = 0$ spin structure [44]. Even if $D_z = 0$, the coplanar structure can be equally stabilized by the NNN coupling J_2 [53]. Depending on the sign of D_z , two vector chiralities can be allowed in the kagome lattice. As shown in Fig. 2, we choose that $D_z > 0$ corresponds to the positive vector chirality in the Ref. 44. The in-plane DMI D_p breaks mirror reflection symmetry with respect to the kagome plane and the global spin rotation symmetry [44, 45]. It prefers umbrella spins. However, the vector chirality that stems from the in-plane component D_p is the same as the one selected by $D_z > 0$. By taking spin \mathbf{S}_i as a classical vector, the canting angle of the 120° spin structure up to the first order can be

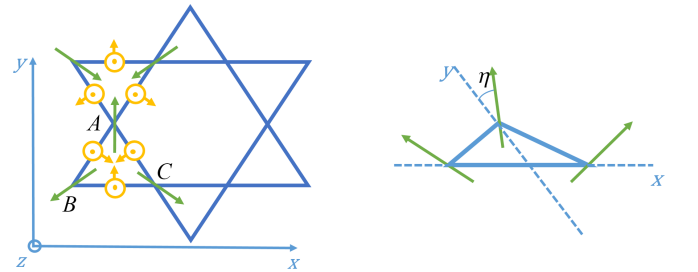


FIG. 2. Non-coplanar spin configuration on the kagome lattice with positive vector chirality. All the spins have a weak z component resulting in weak ferromagnetic angle η . The yellow arrows and circles in the middle point between the magnetic sites represent the in-plane DMI and out-plane DMI, respectively.

expressed by (see the Appendix A for details),

$$\eta = \frac{B/S + 2\sqrt{3}D_p}{6(J_1 + J_2) + 2\sqrt{3}D_z}. \quad (9)$$

For a small η , Eq. (9) is a good approximation. It is obvious that one can eliminate the canting angle to recover the coplanar spin structure by balancing the in-plane DMI with applied external magnetic field $B = -2\sqrt{3}SD_p$. Consequently, we have a very good opportunity to check immediately whether the dynamic $\delta\chi_{ijk}$ (but with $\chi_{ijk} = 0$) can result in topological magnon bands or not.

The spin wave excitations of the 120° coplanar $\mathbf{q} = 0$ spin structure with balanced D_p and B is investigated by Holstein-Primakoff bosons (see Appendix A). Figure 3 shows the bulk magnon bands along the high-symmetry points of the Brillouin zone with $\Gamma = (0, 0)$, $\mathbf{K} = (2\pi/3, 0)$, and $\mathbf{M} = (\pi/2, \pi/2\sqrt{3})$. The parameters are from the ideal kagome antiferromagnets such as iron jarosite $\text{KFe}_3(\text{OH})_6(\text{SO}_4)_2$ [45] and veseignite $\text{BaCu}_3\text{V}_2\text{O}_8(\text{OH})_2$ [54]. There are two evident features in the figures: (i) One Goldstone mode at the Γ point due to regaining of the $\text{SO}(2)$ rotation symmetry by adjusting magnetic field B to compensate the canting angle induced by the in-plane D_p . (ii) Finite gap appears in the rest of the Brillouin zone. It should be noted that these gaps do not go to zero in the thermodynamic limit even if they look very small.

In general, the dynamic $\delta\chi_{ijk}$ is composed of three main contributions,

$$H^\Phi = H_{J_1}^\Phi + H_{D_z}^\Phi + H_{D_p}^\Phi, \quad (10)$$

$$H_{J_1}^\Phi = -J_1 \frac{\sqrt{3}}{2} \sin \eta \hat{\mathbf{z}} \cdot (\mathbf{S}'_i \times \mathbf{S}'_j), \quad (11)$$

$$H_{D_z}^\Phi = D_z \frac{1}{2} \sin \eta \hat{\mathbf{z}} \cdot (\mathbf{S}'_i \times \mathbf{S}'_j), \quad (12)$$

$$H_{D_p}^\Phi = D_p \frac{1}{2} \cos \eta \hat{\mathbf{z}} \cdot (\mathbf{S}'_i \times \mathbf{S}'_j). \quad (13)$$

The corresponding fictitious magnetic flux reads $K_\Phi \sim (-J_1\sqrt{3}\sin\eta + D_z\sin\eta + D_p\cos\eta)$, which is closely coupled to the z -polarized (magnon) spin current [38]. Evidently, the dynamic scalar chirality $\delta\chi_{ijk}$ survives even at $\eta = 0$. Now the in-plane DMI becomes an only source of topological spin excitations in the $\mathbf{q} = 0$ coplanar magnetic ordering, which possesses different mechanism from the one with non-coplanar magnetic configuration induced by external magnetic fields [39, 40]. Furthermore, the $H_{D_p}^\Phi$ won't disappear immediately even if the coplanar spins are deformed into the umbrella configuration. The influence of the in-plane DMI on the magnon bands of non-coplanar configuration will be discussed in Sec. IV.

In order to confirm the topological nature of magnons, the chiral edge states are demonstrated in the Fig. 4 using the strip geometry with open boundary conditions along y direction and infinite along x direction. We clearly see

crossed chiral edge modes between the middle and lower bands from Fig. 4 (a) and (b). This forcefully supports the existence of topological magnons driven by only the in-plane DMI. Another evidentiary quality of topological magnons is the non-zero Chern number of the bulk bands. Unlike electron systems, the Chern number of bosonic systems is not well-defined because of the lack of the Fermi surface and an evenly filled band. However, we can still calculate the Chern number for the n -th bulk band mathematically as

$$C_n = \frac{1}{2\pi} \int_{BZ} \Omega_{n\mathbf{k}} d^2\mathbf{k}, \quad (14)$$

where $\Omega_{n\mathbf{k}}$ is the Berry curvature for bosonic Bogliubov-de Gennes systems. Noted that the formula of $\Omega_{n\mathbf{k}}$ has to be modified accordingly (See Appendix B) [55]. The Chern numbers in Fig. 3 (a) and (b) are given as $(+3, -1, -2)$ going from the lower, middle, and upper bands. When the D_p drops to zero, both the gapless chiral edge modes and the Chern numbers will disappear. This is insofar conclusive: the non-trivial topological spin excitations of coplanar magnetic structures must be purely tied to the dynamic spin chirality given by the in-plane DMI (cf. also Eq. (7)). For comparison, the edge modes under the influence of D_p with the large canting angle $\sin\eta = 0.4$ are also shown in Fig. 4 (c), which is almost as same as the case without D_p in Ref. [40]. This seemingly suggests that the D_p is negligible for the topological property of the non-coplanar spin configuration as in the previous studies [40] when the canting angle η is quite large. However, one should be careful about this conclusion because the Chern number is the feature of the entire Brillouin zone. Actually, the calculations show that the Chern number $C_n = (-1, +2, -1)$ for magnon bands with D_p is different from $C_n = (-1, +4, -3)$ for the bands in the absence of D_p . The change of Chern numbers stems from the symmetry breaking. As we mentioned, D_p breaks the $\text{SO}(2)$ spin rotation symmetry and tends to give rise to weak out-of-plane ferromagnetic component. As a result, the zero-energy Goldstone mode at the Γ point is lifted in the non-coplanar spins by the in-plane DMI. A new gap at the Γ point increases with the external field B . The “monopole” at the Γ - \mathbf{K} line is dissolved as the magnetic field B reaches the threshold value. In Figure 5, we demonstrate the substantial change happening in the magnon band structures and Berry curvature of the non-coplanar spins with/without D_p .

IV. TOPOLOGICAL THERMAL HALL EFFECT

The thermal Hall effect is a powerful probe to unveil the topological nature of low-energy quasiparticle excitations in magnetic systems. The magnon thermal Hall conductivity κ_{xy} is closely connected to the Berry curva-

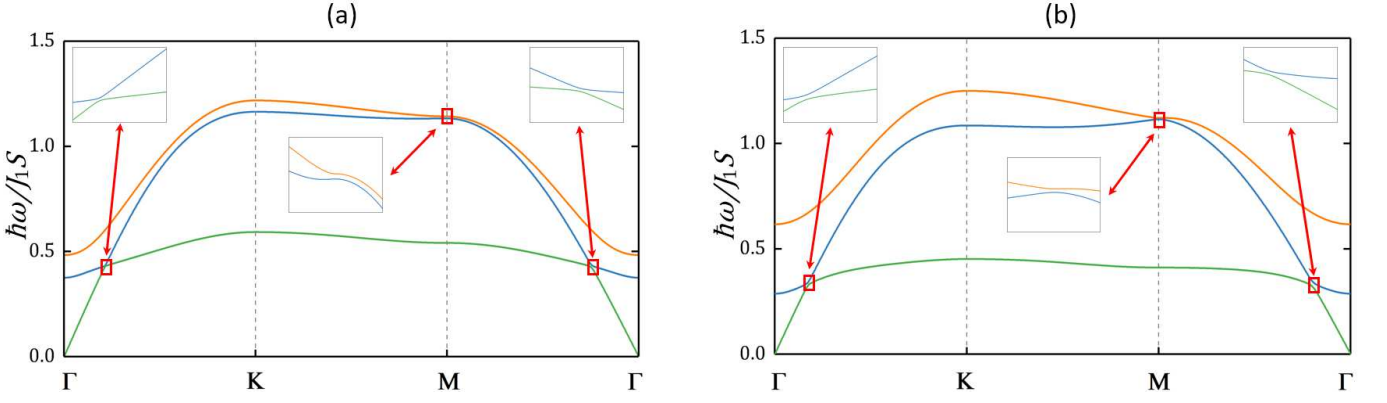


FIG. 3. The magnon bulk bands of the coplanar spin configuration with the canting angular $\eta = 0$. (a) $D_z/J_1 = 0.062$, $D_p/J_1 = 0.062$, $J_2/J_1 = 0.035$, and $B/J_1 = -0.537$ with $J_1 = 3.18$ meV corresponding to iron jarosite $\text{KFe}_3(\text{OH})_6(\text{SO}_4)_2$. (b) $D_z/J_1 = 0.07$, $D_p/J_1 = 0.19$, $J_2/J_1 = 0$, and $B/J_1 = -0.329$ with $J_1 = 4.6$ meV corresponding to veseignite $\text{BaCu}_3\text{V}_2\text{O}_8(\text{OH})_2$. The insets magnify the gaps of magnon bands indicated by red squares.

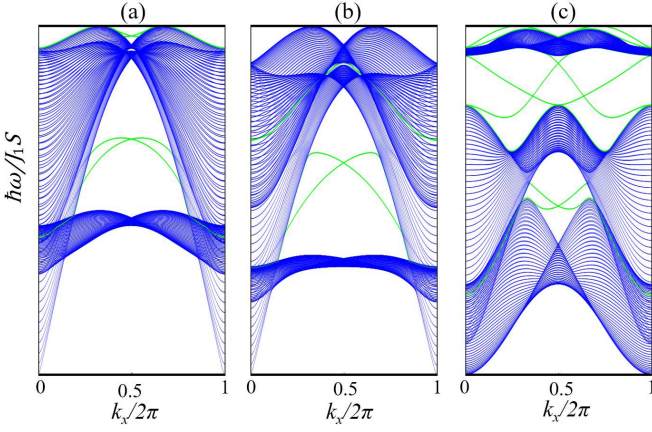


FIG. 4. Edge states in kagome antiferromagnets with in-plane DMI. (a) $\eta = 0$, parameters corresponding to iron jarosite $\text{KFe}_3(\text{OH})_6(\text{SO}_4)_2$ (same as in Fig. 3(a)). (b) $\eta = 0$, parameters corresponding to veseignite $\text{BaCu}_3\text{V}_2\text{O}_8(\text{OH})_2$ (same as in Fig. 3(b)). (c) $\sin \eta = 0.4$, $D_z/J_1 = 0.06$, $D_p/J_1 = 0.06$, and $J_2/J_1 = 0.03$ corresponding to the parameters in Ref. [40] with in-plane DMI appended. The blue lines are the gapped bulk bands and the green lines are the gapless edge modes.

ture [23],

$$\kappa_{xy} = -\frac{k_B^2 T}{\hbar V} \sum_{\mathbf{k} \in BZ} \sum_{n=1}^N \left\{ c_2[g(\varepsilon_{n\mathbf{k}})] - \frac{\pi^2}{3} \right\} \Omega_{n\mathbf{k}}. \quad (15)$$

Here, $g(\varepsilon_{n\mathbf{k}})$ is the Bose distribution function $g(\varepsilon_{n\mathbf{k}}) = 1/[\exp(\varepsilon_{n\mathbf{k}}/k_B T) - 1]$, $c_2(x)$ is defined as $c_2(x) = (1+x)(\ln \frac{1+x}{x})^2 - (\ln x)^2 - 2\text{Li}_2(-x)$. The (low) temperature dependence of κ_{xy} of the coplanar spin configuration is plotted in Figure 6 with the parameters of $\text{KFe}_3(\text{OH})_6(\text{SO}_4)_2$ and $\text{BaCu}_3\text{V}_2\text{O}_8(\text{OH})_2$, respectively. Both showing monotonically increasing behaviour, very similar to the previous temperature dependence of the non-coplanar configuration caused by D_p in Ref. [41].

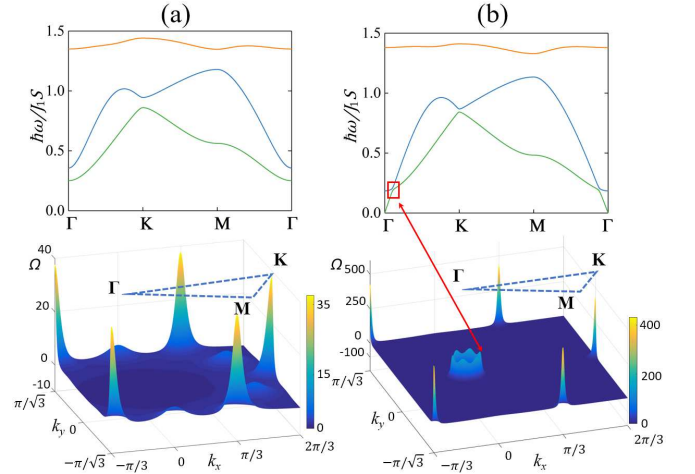


FIG. 5. The magnon bulk bands (upper) and the corresponding Berry curvature of the middle band (bottom). (a) $D_p/J_1 = 0.06$. (b) $D_p/J_1 = 0$. Other parameters are the same as in Fig. 4(c). The “monopole” at the Γ -K line is indicated by the red square.

That means that the in-plane DMI dominates the Hall-type spin transport in the system even if there is a small canting angle. However, while the canting angle increases with D_p (cf. Eq. (9)), the role of the in-plane DMI on κ_{xy} of the non-coplanar spin configures is complex as shown in the following.

A. Small canting angle

As given in the Eq. (10), the fictitious magnetic flux K_ϕ is composed of three main contributions as $\eta \neq 0$. When the canting angle η is smaller than about 0.1, we have $H_{D_p}^\Phi \sim D_p(1 - \eta^2)$, $H_{J_1}^\Phi \sim J_1\eta$, and $H_{D_z}^\Phi \sim D_z\eta$ (which is one order less than $H_{J_1}^\Phi$ given that the out-of-plane

$D_z/J_1 < 0.1$). The topological properties are now determined by both the non-zero scalar chirality χ_{ijk} (mainly through $H_{J_1}^\Phi$) and the dynamic fluctuation $\delta\chi_{ijk}$ (principally from $H_{D_p}^\Phi$). Moreover, when the canting angle is very small ($\eta \approx 0$), the dynamic $\delta\chi_{ijk}$ becomes the dominant mechanism of topological magnon bands. So it is not strange that one can still have a large thermal Hall effect even the scalar chirality $\chi_{ijk} \approx 0$. On the other hand, to exclude a phononic contribution from the thermal transport, the sign changes in κ_{xy} induced by the Chern number (K_Φ) sign alternation is incisive when varying the external magnetic field. Such the phase transition point can be estimated based on the Eq. (9) and Eq. (10),

$$\begin{aligned} K_\Phi &\sim J_1\sqrt{3}\eta - D_z\eta - D_p(1 - \eta^2) \\ &= \alpha \cdot B/S + \beta + \mathcal{O}(B^2), \\ \alpha &= \frac{\sqrt{3}J_1 - D_z}{6(J_1 + J_2) + 2\sqrt{3}D_z}; \\ \beta &= \left(\frac{6J_1 - 2\sqrt{3}D_z}{6(J_1 + J_2) + 2\sqrt{3}D_z} - 1 \right) D_p. \end{aligned} \quad (16)$$

Figure 7 indicates the critical value of magnetic field, $B/J_1S \sim 0.0235$ (i.e., $B/J_1 \sim 0.0588$ with $S = \frac{5}{2}$) with the parameters of $\text{KFe}_3(\text{OH})_6(\text{SO}_4)_2$, which is in consistent with the numerical result ($B/J_1 \sim 0.06$) [41]. Given that $J_1 = 3.18$ meV, κ_{xy} undergoes sign changes at $B \sim 1.6$ Tesla, which can in turn be used for valuing the strength of the in-plane DMI of the frustrated kagome antiferromagnets.

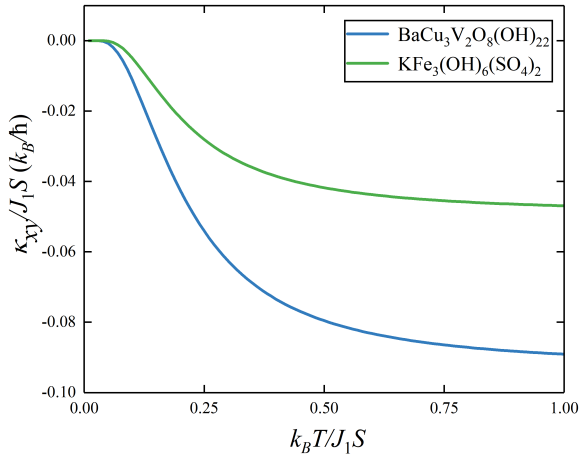


FIG. 6. Low temperature dependence of thermal Hall conductivity κ_{xy} with the canting angle $\eta = 0$.

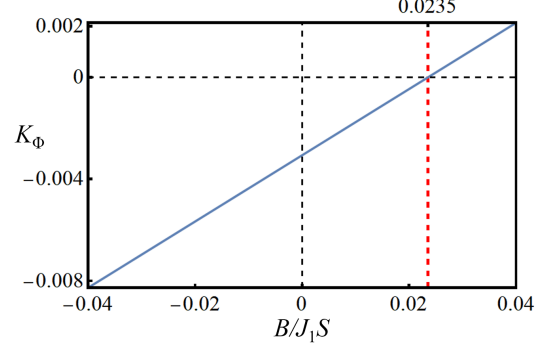


FIG. 7. The flux K_Φ as a function of applied magnetic field B based on Eq. (16) with the parameters of $\text{KFe}_3(\text{OH})_6(\text{SO}_4)_2$.

B. Large canting angle

For the non-coplanar umbrella spins with large canting angle ($\cos \eta \ll 1$), Eq. (10) indicates that the contribution of the in-plane DMI $H_{D_p}^\Phi$ is tiny compared to the $H_{J_1}^\Phi$ and $H_{D_z}^\Phi$. It seems that the effect of $H_{D_p}^\Phi$ on the magnon topological properties could be negligible. However, it is not true from the point view of spin symmetry. As shown in Fig. 5, the in-plane D_p breaks the global spin rotation symmetry and results in a finite gap at the Γ point. We have then fully gapped magnon bands in the entire Brillouin zone, which provides an energy barrier for thermal excitations. Thus, it is anticipated that the thermal Hall conductivity with the in-plane DMI will be smaller than the value without D_p , as indicated by the c_2 function as well [23]. Figure 8 displays the comparison of κ_{xy} with/without D_p under the large canting angle, respectively. As expected, the presence of in-plane DMI blocks the excitations and suppresses the thermal Hall effect.

V. CONCLUSIONS

In summary, we have shown that the fluctuation of scalar spin chirality $\delta\chi_{ijk}$ is directly related to the magnonic transport in spin systems. For the magnetically ordered system with nonzero $\delta\chi_{ijk}$ and fictitious magnetic flux K_Φ in terms of the DMI, the time-reversal symmetry is dynamically broken and topologically non-trivial bands of magnons can be expected. Based on these considerations and detail analysis for the frustrated kagome antiferromagnets with the in-plane DMI, it was found that the in-plane DMI can give rise to topological magnon bands with chiral edge modes and non-zero Chern number even in the case of coplanar $\mathbf{q} = 0$ Néel state. The proposed model has been applied to real antiferromagnets to discuss the effects of in-plane DMI on the magnon thermal Hall responses and resolve the con-

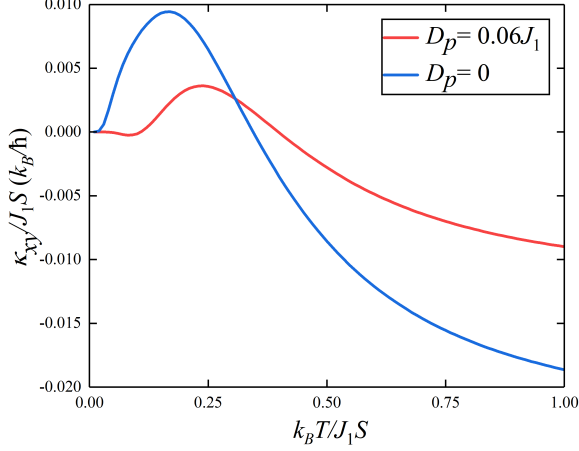


FIG. 8. Low temperature dependence of thermal Hall conductivity κ_{xy} with $\sin \eta = 0.4$, $D_z/J_1 = 0.06$, and $J_2/J_1 = 0.03$.

tradiictory of large thermal Hall conductivities but with

tiny spin chirality. For the non-coplanar spins with large canting angle η , the gapped magnons induced by the in-plane DMI is considerably suppressed the thermal excitations and reduces the thermal Hall conductivity κ_{xy} . In this regard, the present study generalises the *No-go* theorem for the antiferromagnetically coupled systems and clarifies the mechanism of nontrivial topology in magnon systems.

VI. ACKNOWLEDGMENTS

This work is supported by the National Natural Science Foundation of China (No. 11474138 and No. 11834005), the German Research Foundation (No. SFB 762), the Program for Changjiang Scholars and Innovative Research Team in University (No. IRT-16R35), the Fundamental Research Funds for the Central Universities, Ministry of Science and Technology of China through grants CN-SK-8-4, the Slovak Academy of Sciences (Grant No. 2/0059/17) and the Slovak Research and Development Agency (APVV SK-CN-2017-0004).

Appendix A: The magnon tight binding Hamiltonian in the Holstein-Primakoff mean-field theory

To study the fluctuations of the spin wave, we first need to determine the classical groundstate of the system. In the classical limit, the $SU(2)$ spin operators can be replaced by the classical $SO(3)$ vectors, $\mathbf{S} = S(\cos \theta \cos \eta, \sin \theta \cos \eta, \sin \eta)$, where η is the canting angle. The oriented angles of three sub-lattices are $\theta_A = \pi/2$, $\theta_B = 7\pi/6$, $\theta_C = -\pi/6$ for the 120° magnetic configuration. Thus, the classical energy reads [44]

$$\frac{E^{cl}}{NS^2} = (J_1 + J_2)(1 - 3 \cos 2\eta)/2 - \sqrt{3}D_z \cos^2 \eta - \sqrt{3}D_p \sin 2\eta - B \sin \eta/S. \quad (A1)$$

By minimizing the energy, the canting angle η is determined by,

$$0 = \frac{\partial}{\partial \eta} \left(\frac{E^{cl}}{NS^2} \right) = 3(J_1 + J_2) \sin 2\eta + \sqrt{3}D_z \sin 2\eta - 2\sqrt{3}D_p \cos 2\eta - B \cos \eta/S. \quad (A2)$$

Up to the first order, η is given by

$$\eta \approx \frac{B/S + 2\sqrt{3}D_p}{6(J_1 + J_2) + 2\sqrt{3}D_z}. \quad (A3)$$

For the magnonic properties, it is necessary to perform a local coordinate transformation for getting the spin-wave excitation above the groundstate,

$$\begin{aligned} \mathbf{S}_A &= (S'_A{}^x, \cos \eta S'_A{}^z + \sin \eta S'_A{}^y, -\cos \eta S'_A{}^y + \sin \eta S'_A{}^z), \\ \mathbf{S}_B &= \left(-\frac{1}{2}S'_B{}^x - \frac{\sqrt{3}}{2}(\cos \eta S'_B{}^z + \sin \eta S'_B{}^y), \frac{\sqrt{3}}{2}S'_B{}^x - \frac{1}{2}(\cos \eta S'_B{}^z + \sin \eta S'_B{}^y), -\cos \eta S'_B{}^y + \sin \eta S'_B{}^z \right), \\ \mathbf{S}_C &= \left(-\frac{1}{2}S'_C{}^x + \frac{\sqrt{3}}{2}(\cos \eta S'_C{}^z + \sin \eta S'_C{}^y), -\frac{\sqrt{3}}{2}S'_C{}^x - \frac{1}{2}(\cos \eta S'_C{}^z + \sin \eta S'_C{}^y), -\cos \eta S'_C{}^y + \sin \eta S'_C{}^z \right), \end{aligned} \quad (A4)$$

where \mathbf{S}'_i is the local spin operator, (A, B, C) are three sublattice sites as depicted in Fig. 2. Then the Hamiltonian Eq. (8) can be rewritten as

$$H = H_{J_1} + H_{J_2} + H_{D_z} + H_{D_p} + H_z, \quad (\text{A5})$$

$$H_{J_1} = J_1 \sum_{\langle ij \rangle} \left[\cos \frac{2}{3} \pi \mathbf{S}'_i \cdot \mathbf{S}'_j - \sin \frac{2}{3} \pi \sin \eta \hat{\mathbf{z}} \cdot (\mathbf{S}'_i \times \mathbf{S}'_j) + 2 \sin^2 \frac{1}{3} \pi (\cos^2 \eta S'^y_i S'^y_j + \sin^2 \eta S'^z_i S'^z_j) \right], \quad (\text{A6})$$

$$H_{J_2} = J_2 \sum_{\langle\langle ij \rangle\rangle} \left[\cos \frac{2}{3} \pi \mathbf{S}'_i \cdot \mathbf{S}'_j - \sin \frac{2}{3} \pi \sin \eta \hat{\mathbf{z}} \cdot (\mathbf{S}'_i \times \mathbf{S}'_j) + 2 \sin^2 \frac{1}{3} \pi (\cos^2 \eta S'^y_i S'^y_j + \sin^2 \eta S'^z_i S'^z_j) \right], \quad (\text{A7})$$

$$H_{D_z} = -D_z \sum_{\langle ij \rangle} \left[\sin \frac{2}{3} \pi (S'^x_i S'^x_j + \sin^2 \eta S'^y_i S'^y_j + \cos^2 \eta S'^z_i S'^z_j) + \cos \frac{2}{3} \pi \sin \eta \hat{\mathbf{z}} \cdot (\mathbf{S}'_i \times \mathbf{S}'_j) \right], \quad (\text{A8})$$

$$H_{D_p} = -D_p \sum_{\langle ij \rangle} \left[\sin \frac{2}{3} \pi \sin 2\eta (S'^z_i S'^z_j - S'^y_i S'^y_j) + \cos \frac{2}{3} \pi \cos \eta \hat{\mathbf{z}} \cdot (\mathbf{S}'_i \times \mathbf{S}'_j) \right], \quad (\text{A9})$$

$$H_z = -B \sin \eta \sum_i S'^z_i. \quad (\text{A10})$$

Obviously, several terms that can be rewritten as the fictitious magnetic field coupling with spin chirality provide anomalous velocity of the magnons, they are

$$H^\Phi = \left(-J_1 \frac{\sqrt{3}}{2} \sin \eta + \frac{D_z}{2} \sin \eta + \frac{D_p}{2} \cos \eta \right) \hat{\mathbf{z}} \cdot (\mathbf{S}'_i \times \mathbf{S}'_j). \quad (\text{A11})$$

We have neglected the flux term coming from H_{J_2} . Because the magnitude of $J_2 \sin \eta$ is far less than $J_1 \sin \eta$ and $D_p \cos \eta$ under the condition of small canting angle η .

Following the Holstein-Primakoff approach, the local spin operators are expressed by the bosonic annihilation and creation operators as $S'^x_i = \sqrt{S/2}(b_i^\dagger + b_i)$, $S'^y_i = i\sqrt{S/2}(b_i^\dagger - b_i)$, and $S'^z_i = S - b_i^\dagger b_i$ [56]. The magnon tight binding Hamiltonian becomes

$$H_{SW} = S \sum_{\mathbf{k}, \alpha, \beta; 1, 2} 2 (M_{\alpha\beta}^0 \delta_{\alpha\beta} + M_{\alpha\beta; 1, 2}) b_{\mathbf{k}\alpha}^\dagger b_{\mathbf{k}\beta} + M'_{\alpha\beta; 1, 2} (b_{\mathbf{k}\alpha}^\dagger b_{-\mathbf{k}\beta}^\dagger + b_{\mathbf{k}\alpha} b_{-\mathbf{k}\beta}), \quad (\text{A12})$$

where $\alpha, \beta = A, B, C$ and the coefficient matrixs are expressed by $\mathbf{M}^0 = M^0 \mathbf{I}_{3 \times 3}$ with $M^0 = (J_1 + J_2)(1 - 3 \sin^2 \eta) + D_z \sqrt{3} \cos^2 \eta + D_p \sqrt{3} \sin 2\eta + B \sin \eta / 2S$.

$$\mathbf{M}_{1,2} = M_{1,2} \begin{pmatrix} 0 & \gamma_{AB}^{1,2} e^{-i\phi_{1,2}} & \gamma_{CA}^{1,2} e^{i\phi_{1,2}} \\ \gamma_{AB}^{*1,2} e^{i\phi_{1,2}} & 0 & \gamma_{BC}^{1,2} e^{-i\phi_{1,2}} \\ \gamma_{CA}^{*1,2} e^{-i\phi_{1,2}} & \gamma_{BC}^{*1,2} e^{i\phi_{1,2}} & 0 \end{pmatrix} \quad \text{and} \quad \mathbf{M}'_{1,2} = M'_{1,2} \begin{pmatrix} 0 & \gamma_{AB}^{1,2} & \gamma_{CA}^{1,2} \\ \gamma_{AB}^{*1,2} & 0 & \gamma_{BC}^{1,2} \\ \gamma_{CA}^{*1,2} & \gamma_{BC}^{*1,2} & 0 \end{pmatrix}, \quad (\text{A13})$$

where $\gamma_{AB}^1 = \cos k_1$, $\gamma_{BC}^1 = \cos k_2$, $\gamma_{CA}^1 = \cos k_3$; $\gamma_{AB}^2 = \cos p_1$, $\gamma_{BC}^2 = \cos p_2$, $\gamma_{CA}^2 = \cos p_3$ and $p_i = \mathbf{p} \cdot \mathbf{e}'_i$, $\mathbf{e}'_1 = \mathbf{e}_3 - \mathbf{e}_2$, $\mathbf{e}'_2 = \mathbf{e}_1 - \mathbf{e}_3$, $\mathbf{e}'_3 = \mathbf{e}_2 - \mathbf{e}_1$. The normalized fluxes are given by $\phi_{1,2} = \tan^{-1}(M_{1,2}^{im}/M_{1,2}^e)$, and $M_{1,2} = \sqrt{(M_{1,2}^e)^2 + (M_{1,2}^{im})^2}$, where

$$M_1^e = \frac{1}{4} J_1 (3 \cos^2 \eta - 2) - \frac{\sqrt{3}}{4} D_z (1 + \sin^2 \eta) + \frac{\sqrt{3}}{4} D_p \sin 2\eta, \quad (\text{A14})$$

$$M_1^{im} = \left(-\frac{\sqrt{3}}{2} J_1 + \frac{1}{2} D_z \right) \sin \eta + \frac{1}{2} D_p \cos \eta, \quad (\text{A15})$$

$$M'_1 = \frac{1}{4} (3J_1 \cos^2 \eta + \sqrt{3} D_z \cos^2 \eta + \sqrt{3} D_p \sin 2\eta), \quad (\text{A16})$$

$$M_2^e = \frac{1}{4} J_2 (3 \cos^2 \eta - 2), \quad (\text{A17})$$

$$M_2^{im} = -\frac{\sqrt{3}}{2} J_2 \sin \eta. \quad (\text{A18})$$

It needs to be emphasized that the flux does not vanish even if both η and D_z are equal to zero. This means that the only D_p with coplanar spin structure can break the TRS as well.

By introducing Nambu spinor

$$\begin{bmatrix} \beta_{\mathbf{k}}^\dagger & \beta_{-\mathbf{k}} \end{bmatrix} \equiv \begin{bmatrix} b_{\mathbf{k}A}^\dagger, & b_{\mathbf{k}B}^\dagger, & b_{\mathbf{k}C}^\dagger, & b_{-\mathbf{k}A}, & b_{-\mathbf{k}B}, & b_{-\mathbf{k}C} \end{bmatrix}, \quad (\text{A19})$$

The Hamiltonian can be written as

$$H_{SW} = E_0 + S \sum_{\mathbf{k}} \begin{bmatrix} \beta_{\mathbf{k}}^\dagger & \beta_{-\mathbf{k}} \end{bmatrix} \cdot \mathbf{H}_{\mathbf{k}} \cdot \begin{bmatrix} \beta_{\mathbf{k}} \\ \beta_{-\mathbf{k}}^\dagger \end{bmatrix}. \quad (\text{A20})$$

Appendix B: Berry curvature for bosonic Bogliubov-de Gennes systems

Although the Chern number can be still defined as Eq. (14) for the bosonic BdG system, the formula of Berry curvature is different from the fermion system. A general formalism is developed for bosonic BdG systems by Shindou [55]. Unfortunately, this method contains derivatives of the eigenstates that can not be used directly for numerical calculations. Here the gauge-independent formula of Berry curvature are provided for bosonic BdG systems. We consider a quadratic form of generic bosonic Hamiltonian as given by Eq. (A20). Such a bosonic BdG Hamiltonian can be diagonalized by the Bogliubov transformation by using the para-unitary transformation $\mathcal{T}_{\mathbf{k}}$ instead of the unitary transformation,

$$\mathcal{T}_{\mathbf{k}}^\dagger \mathbf{H}_{\mathbf{k}} \mathcal{T}_{\mathbf{k}} = \begin{bmatrix} E_{\mathbf{k}} & \\ & E_{-\mathbf{k}} \end{bmatrix} \quad (\text{B1})$$

with $[\gamma_{\mathbf{k}}^\dagger, \gamma_{-\mathbf{k}}] \mathcal{T}_{\mathbf{k}}^\dagger = [\beta_{\mathbf{k}}^\dagger, \beta_{-\mathbf{k}}]$, whose diagonal element gives the dispersion relations of the bulk bands. The matrix \mathcal{T} satisfies the para-unitary

$$\mathcal{T}^\dagger \hat{\tau} \mathcal{T} = \hat{\tau}, \quad (\text{B2})$$

where a diagonal matrix $\hat{\tau}$ takes ± 1 in the particle/hole space, i.e., $[\tau]_{jm} = \delta_{jm} \tau_j$ with $\tau_j = +1$ for $j = 1, \dots, N$ and $\tau_j = -1$ for $N+1, \dots, 2N$. N is the number of bands. The paraunitary defines the Berry Curvature of α bulk energy band given by,

$$\begin{aligned} \Omega_{ij;\alpha} &= -2\text{Im} [\hat{\tau}(\partial_i \mathcal{T}^\dagger) \hat{\tau}(\partial_j \mathcal{T})]_{\alpha\alpha} \\ &= -2\text{Im} [\tau_{\alpha\alpha}(\partial_i \mathcal{T}_\alpha^\dagger) \hat{\tau}(\partial_j \mathcal{T}_\alpha)] \\ &= -2\text{Im} [\tau_{\alpha\alpha} \langle \partial_i \mathcal{T}_\alpha^\dagger | \hat{\tau} \partial_j \mathcal{T}_\alpha \rangle]. \end{aligned} \quad (\text{B3})$$

Using Eq. (B1) and Eq. (B2), the completeness operator is derived as

$$\sum_{\beta}^{2N} \tau_{\beta\beta} |\hat{\tau} \mathcal{T}_\beta\rangle \langle \mathcal{T}_\beta^\dagger| = \mathbf{I}_{2N \times 2N}, \quad (\text{B4})$$

$$\sum_{\beta}^{2N} \tau_{\beta\beta} |\hat{\tau} \mathcal{T}_\beta\rangle \langle \mathcal{T}_\beta^\dagger| |\hat{\tau} \mathcal{T}_\alpha\rangle = |\hat{\tau} \mathcal{T}_\alpha\rangle. \quad (\text{B5})$$

Insert Eq. (B4) into Eq. (B3), we have

$$\begin{aligned} \langle \mathcal{T}_\beta^\dagger | H | \mathcal{T}_\alpha \rangle &= \langle \mathcal{T}_\beta^\dagger | E_\alpha \hat{\tau} | \mathcal{T}_\alpha \rangle, \\ \langle \partial_j \mathcal{T}_\beta^\dagger | H | \mathcal{T}_\alpha \rangle + \langle \mathcal{T}_\beta^\dagger | \partial_j H | \mathcal{T}_\alpha \rangle + \langle \mathcal{T}_\beta^\dagger | H | \partial_j \mathcal{T}_\alpha \rangle &= \langle \partial_j \mathcal{T}_\beta^\dagger | E_\alpha \hat{\tau} | \mathcal{T}_\alpha \rangle + \langle \mathcal{T}_\beta^\dagger | \partial_j E_\alpha \hat{\tau} | \mathcal{T}_\alpha \rangle + \langle \mathcal{T}_\beta^\dagger | E_\alpha \hat{\tau} | \partial_j \mathcal{T}_\alpha \rangle, \\ \langle \mathcal{T}_\beta^\dagger | \partial_j H | \mathcal{T}_\alpha \rangle &= \langle \mathcal{T}_\beta^\dagger | \hat{\tau} \partial_j \mathcal{T}_\alpha \rangle (E_\alpha - E_\beta), \\ \langle \mathcal{T}_\beta^\dagger | \hat{\tau} \partial_j \mathcal{T}_\alpha \rangle &= \langle \mathcal{T}_\beta^\dagger | \partial_j H | \mathcal{T}_\alpha \rangle / (E_\alpha - E_\beta). \end{aligned} \quad (\text{B6})$$

Then the Berry curvature can be written alternatively as:

$$\Omega_{ij;\alpha} = -2\text{Im} \left[\tau_{\alpha\alpha} \sum_{\beta \neq \alpha}^{2N} \tau_{\beta\beta} \frac{\langle \mathcal{T}_\alpha^\dagger | \partial_i H | \mathcal{T}_\beta \rangle \langle \mathcal{T}_\beta^\dagger | \partial_j H | \mathcal{T}_\alpha \rangle}{(E_\alpha - E_\beta)^2} \right]. \quad (\text{B7})$$

We can immediately see that Eq. (B7) is manifestly gauge independent. It is more advantageous to use Eq. (B7) to replace the Eq. (B3) as the Berry curvature does not depend explicitly on the phases of eigenvector. Obviously, the Berry curvature and the Chern number calculated by the Eq. (B7) are in accord with the relations,

$$\sum_{\alpha=1}^N C_{\alpha} = \sum_{\alpha=N+1}^{2N} C_{\alpha} = 0, \quad (\text{B8})$$

$$\Omega_{ij;\alpha}(\mathbf{k}) = -\Omega_{ij;\alpha+N}(-\mathbf{k}) \quad (\text{B9})$$

as derived in Ref. [55].

-
- [1] F. D. M. Haldane, Phys. Rev. Lett. **61**, 2015 (1988).
[2] C. L. Kane and E. J. Mele, Phys. Rev. Lett. **95**, 146802 (2005).
[3] M. Z. Hasan and C. L. Kane, Rev. Mod. Phys. **82**, 3045 (2010).
[4] P. Roushan, J. Seo, C. V. Parker, Y. S. Hor, D. Hsieh, D. Qian, A. Richardella, M. Z. Hasan, R. J. Cava, and A. Yazdani, Nature **460**, 1106 (2009).
[5] X.-L. Qi and S.-C. Zhang, Rev. Mod. Phys. **83**, 1057 (2011).
[6] N. Nagaosa, J. Sinova, S. Onoda, A. H. MacDonald, and N. P. Ong, Rev. Mod. Phys. **82**, 1539 (2010).
[7] D. Xiao, M.-C. Chang, and Q. Niu, Rev. Mod. Phys. **82**, 1959 (2010).
[8] L. Lu, J. D. Joannopoulos, and M. Soljačić, Nature Publishing Group, 1 (2014).
[9] A. B. Khanikaev and G. Shvets, Nature Photon **11**, 763 (2017).
[10] T. Ozawa, H. M. Price, A. Amo, N. Goldman, M. Hafezi, L. Lu, M. Rechtsman, D. Schuster, J. Simon, O. Zilberberg, and others, arXiv preprint arXiv:1802.04173 (2018).
[11] C. Strohm, G. L. J. A. Rikken, and P. Wyder, Phys. Rev. Lett. **95**, 155901 (2005).
[12] C. L. Kane and T. C. Lubensky, Nat Phys **10**, 39 (2013).
[13] B. G.-g. Chen, N. Upadhyaya, and V. Vitelli, Proc. Natl. Acad. Sci. U.S.A. **111**, 13004 (2014).
[14] R. Süssstrunk and S. D. Huber, Science **349**, 47 (2015).
[15] O. Stenull, C. L. Kane, and T. C. Lubensky, Phys. Rev. Lett. **117**, 068001 (2016).
[16] R. Süssstrunk and S. D. Huber, Proc. Natl. Acad. Sci. U.S.A. **113**, E4767 (2016).
[17] H. Katsura, N. Nagaosa, and P. A. Lee, Phys. Rev. Lett. **104**, 066403 (2010).
[18] Y. Onose, T. Ideue, H. Katsura, Y. Shiomi, N. Nagaosa, and Y. Tokura, Science **329**, 297 (2010).
[19] R. Matsumoto and S. Murakami, Phys. Rev. Lett. **106**, 197202 (2011).
[20] T. Ideue, Y. Onose, H. Katsura, Y. Shiomi, S. Ishiwata, N. Nagaosa, and Y. Tokura, Phys. Rev. B **85**, 2993 (2012).
[21] L. Zhang, J. Ren, J.-S. Wang, and B. Li, Phys. Rev. B **87**, 144101 (2013).
[22] A. Mook, J. u. Henk, and I. Mertig, Phys. Rev. B **90**, 024412 (2014).
[23] R. Matsumoto, R. Shindou, and S. Murakami, Phys. Rev. B **89**, 054420 (2014).
[24] M. Hirschberger, R. Chisnell, Y. S. Lee, and N. P. Ong, Phys. Rev. Lett. **115**, 106603 (2015).
[25] R. Chisnell, J. S. Helton, D. E. Freedman, D. K. Singh, R. I. Bewley, D. G. Nocera, and Y. S. Lee, Phys. Rev. Lett. **115**, 147201 (2015).
[26] H. Lee, J. H. Han, and P. A. Lee, Phys. Rev. B **91**, 125413 (2015).
[27] D. Boldrin, B. F. k, M. Enderle, S. Bieri, J. Ollivier, S. Rols, P. Manuel, and A. S. Wills, Phys. Rev. B **91**, 220408 (2015).
[28] S. A. Owerre, J. Phys.: Condens. Matter **28**, 386001 (2016).
[29] S. A. Owerre, Journal of Applied Physics **120**, 043903 (2016).
[30] S. K. Kim, H. e. Ochoa, R. Zarzuela, and Y. Tserkovnyak, Phys. Rev. Lett. **117**, 227201 (2016).
[31] F.-Y. Li, Y.-D. Li, Y. B. Kim, L. Balents, Y. Yu, and G. Chen, Nature Communications **7**, 1 (2016).
[32] A. Mook, J. u. Henk, and I. Mertig, Phys. Rev. Lett. **117**, 157204 (2016).
[33] Y. Su, X. S. Wang, and X. R. Wang, Phys. Rev. B **95**, 224403 (2017).
[34] K. Nakata, S. K. Kim, J. Klinovaja, and D. Loss, Phys. Rev. B **96**, 224414 (2017).
[35] S. A. Owerre, Canadian Journal of Physics **96**, 1216 (2018).
[36] V. Kalmeyer and R. B. Laughlin, Phys. Rev. Lett. **59**, 2095 (1987).
[37] X. G. Wen, F. Wilczek, and A. Zee, Phys. Rev. B **39**, 11413 (1989).
[38] J. H. Han and H. Lee, J. Phys. Soc. Jpn. **86**, 011007 (2017).
[39] S. A. Owerre, J. Phys.: Condens. Matter **29**, 03LT01 (2017).
[40] S. A. Owerre, Phys. Rev. B **95**, 014422 (2017).
[41] P. Laurell and G. A. Fiete, Phys. Rev. B **98**, 094419 (2018).
[42] S. A. Owerre, Journal of Applied Physics **121**, 223904 (2017).
[43] A. Mook, J. Henk, and I. Mertig, Phys. Rev. B **89**, 134409 (2014).
[44] M. Elhajal, B. Canals, and C. Lacroix, Phys. Rev. B **66**, 014422 (2002).
[45] K. Matan, D. Grohol, D. G. Nocera, T. Yildirim, A. B. Harris, S. H. Lee, S. E. Nagler, and Y. S. Lee, Phys. Rev. Lett. **96**, 247201 (2006).
[46] I. Dzyaloshinsky, Journal of Physics and Chemistry of Solids **4**, 241 (1958).
[47] T. o. Moriya, Phys. Rev. **120**, 91 (1960).
[48] O. C 'epas, C. M. Fong, P. W. Leung, and C. Lhuillier, Phys. Rev. B **78**, 140405 (2008).

- [49] L. Messio, O. C. 'epas, and C. Lhuillier, Phys. Rev. B **81**, 064428 (2010).
- [50] Y. Huh, L. Fritz, and S. Sachdev, Phys. Rev. B **81**, 144432 (2010).
- [51] M. Rigol and R. R. P. Singh, Phys. Rev. Lett. **98**, 207204 (2007).
- [52] T. Dodds, S. Bhattacharjee, and Y. B. Kim, Phys. Rev. B **88**, 224413 (2013).
- [53] A. B. Harris, C. Kallin, and A. J. Berlinsky, Phys. Rev. B **45**, 2899 (1992).
- [54] A. Zorko, F. Bert, A. Ozarowski, J. van Tol, D. Boldrin, A. S. Wills, and P. Mendels, Phys. Rev. B **88**, 144419 (2013).
- [55] R. Shindou, R. Matsumoto, S. Murakami, and J.-i. Ohe, Phys. Rev. B **87**, 174427 (2013).
- [56] T. Holstein and H. Primakoff, Phys. Rev. **58**, 1098 (1940).